HIPPOCAMPUS 26:560–576 (2016)

LTP Enhances Synaptogenesis in the Developing Hippocampus

Deborah J. Watson,[1] Linnaea Ostroff,[2] Guan Cao,[1] Patrick H. Parker,[1] Heather Smith,[1] and Kristen M. Harris[1]*

ABSTRACT: In adult hippocampus, long-term potentiation (LTP) produces synapse enlargement while preventing the formation of new small dendritic spines. Here, we tested how LTP affects structural synaptic plasticity in hippocampal area CA1 of Long-Evans rats at postnatal day 15 (P15). P15 is an age of robust synaptogenesis when less than 35% of dendritic spines have formed. We hypothesized that LTP might therefore have a different effect on synapse structure than in adults. Theta-burst stimulation (TBS) was used to induce LTP at one site and control stimulation was delivered at an independent site, both within s. radiatum of the same hippocampal slice. Slices were rapidly fixed at 5, 30, and 120 min after TBS, and processed for analysis by three-dimensional reconstruction from serial section electron microscopy (3DEM). All findings were compared to hippocampus that was perfusion-fixed (PF) *in vivo* at P15. Excitatory and inhibitory synapses on dendritic spines and shafts were distinguished from synaptic precursors, including filopodia and surface specializations. The potentiated response plateaued between 5 and 30 min and remained potentiated prior to fixation. TBS resulted in more small spines relative to PF by 30 min. This TBS-related spine increase lasted 120 min, hence, there were substantially more small spines with LTP than in the control or PF conditions. In contrast, control test pulses resulted in spine loss relative to PF by 120 min, but not earlier. The findings provide accurate new measurements of spine and synapse densities and sizes. The added or lost spines had small synapses, took time to form or disappear, and did not result in elevated potentiation or depression at 120 min. Thus, at P15 the spines formed following TBS, or lost with control stimulation, appear to be functionally silent. With TBS, existing synapses were awakened and then new spines formed as potential substrates for subsequent plasticity. © **2015 The Authors Hippocampus Published by Wiley Periodicals, Inc.**

KEY WORDS: synapses; ultrastructure; 3DEM; postnatal day 15; thetaburst stimulation

INTRODUCTION

Appropriate synaptogenesis and dendritic spine formation during development are necessary for normal cognitive function. Many neurological disorders are characterized by abnormalities that retain juvenile dendritic spines and filopodia (Fiala et al., 2002b; Lin and Koleske, 2010; Penzes et al., 2011; Kuwajima et al., 2013b). Characterizing processes that underlie normal developmental synaptogenesis is vital to understanding the impact of abnormal structure in neurological diseases.

Long-term potentiation (LTP) is a cellular mechanism of learning and memory that is readily induced by theta-burst stimulation (TBS), a pattern that mimics naturally occurring neuronal firing patterns (Staubli and Lynch, 1987; Nguyen and Kandel, 1997; Morgan and Teyler, 2001; Buzsaki, 2002). Synaptic scaling is a homeostatic process that enhances or reduces global synaptic strength after periods of weak or strong activity, respectively (Turrigiano, 2008; Turrigiano, 2012). In adult hippocampal area CA1, the enlargement of some synapses following induction of LTP by TBS is balanced by concurrent suppression of the formation of small dendritic spines (Bourne and Harris, 2011; Bell et al., 2014). These results were the first to show that mature dendrites have a maximal capacity for total synaptic input; they support fewer, larger, and more effective synapses, or more, smaller, and less effective synapses. This balancing of total synaptic input has been named structural synaptic scaling, as it suggests interactions between LTP and homeostatic mechanisms at the structural level.

In hippocampal area CA1 of Long-Evans rats, P12 is the onset age for LTP induced by TBS that lasts for more than 3 h (Cao and Harris, 2012). Consistent with the first appearance of dendritic spines in this brain region, we and others have hypothesized that spine structure facilitates changes in signaling processes leading to enduring LTP (Fiala et al., 1998; Kirov et al., 2004; Bourne and Harris, 2008; Colgan and Yasuda, 2014). By P15, spine density along oblique dendritic branches has reached only 33% of adult levels, whereas by P21 spine density is ~80% of adult levels (Harris et al., 1992; Fiala et al., 2003; Kirov et al., 2004). Thus, P15 is an age of robust synaptogenesis and an important developmental stage to determine whether the structural effects of LTP differ

[1] **Department of Neuroscience, Center for Learning and Memory, Institute for Neuroscience, University of Texas at Austin, Austin, Texas 78731;** [2] **Allen Brain Institute, 551 N 34th St, Seattle, Washington 98103**

Additional Supporting Information may be found in the online version of this article.

Grant sponsor: NIH grants; Grant numbers: NS201184, MH095980, and NS074644 (to K.M.H.) and MH096459 (to D.J.W.); Grant sponsor: Texas Emerging Technologies Fund.

*Correspondence to: Kristen M. Harris, Department of Neuroscience, Center for Learning and Memory, Institute for Neuroscience, University of Texas at Austin, Austin TX 78731, USA. E-mail: kmh2249@gmail.com
D.J.W. and L.O. contributed equally to this work.

Accepted for publication 20 September 2015.
DOI 10.1002/hipo.22536
Published online 29 September 2015 in Wiley Online Library (wileyonlinelibrary.com).

from adults (Bourne and Harris, 2011). For example, LTP induced in the developing hippocampus might facilitate spine formation (unlike adults) or trigger active elimination of redundant synapses (Oh et al., 2015).

Reconstruction in three dimensions through serial section electron microscopy (3DEM) was used to distinguish nonsynaptic filopodia from synaptic dendritic spines, and to measure accurately the spine and synapse densities and dimensions. The results provide new 3DEM data at P15 *in vivo*, and in acute slices following induction of LTP or control test pulse stimulation. The findings show profound contrasts between P15 and mature hippocampus suggesting a basis for new understanding about how the same treatments could result in opposing effects, depending on age.

MATERIALS AND METHODS

All animal use procedures were approved by the Institutional Animal Care and Use Committee at the University of Texas at Austin and complied with the NIH requirements for the humane use of laboratory rats. At the time animals were taken for experimentation, they were all of comparable age (P15-16) and had similar features (weights, open eyes, behaviorally responsive, full bellies, and clean bodies, indicating good maternal care).

Hippocampal Slice Preparation, Stimulation, and Recording

Hippocampal slices (400 μm) were rapidly prepared from P15-16 male Long-Evans rats ($n > 100$, including the initial test experiments), and 2–3 of the very best experiments at each time point were subsequently chosen for 3DEM analyses ($n = 7$, see statistics below). Animals were decapitated, the brain was removed, and the left hippocampus was dissected. Slices were taken from the middle third of the left hippocampus at an angle 70° transverse to the long axis on a tissue chopper (Stoelting, Wood Dale, IL) at room temperature (~25°C) in oxygenated aCSF containing (in mM) 117 NaCl, 5.3 KCl, 26 $NaHCO_3$, 1 NaH_2PO_4, 2.5 $CaCl_2$, 1.3 $MgSO_4$, and 10 D-glucose at pH 7.4. Within 5 min, the slices were transferred to a static–pool interface chamber and were recovered for at least 1 h at 33–34°C on a supporting net at the interface of humidified 95% O_2 and 5% CO_2 atmosphere until recordings began.

Next, a single glass extracellular recording pipette (filled with 120 mM NaCl) was placed in the middle of s. radiatum in area CA1 between two concentric bipolar stimulating electrodes (100 μm outer diameters, Fredrick Haer, Brunswick, ME). Prior work showed that a total separation of ~300–400 μm between the two stimulating electrodes was sufficient to ensure independent activation of subpopulations of synapses (Sorra and Harris, 1998; Ostroff et al., 2002; Bourne and Harris, 2011). Thus, the separation between the two stimulating electrodes was roughly doubled (Fig. 1a).

Stable baseline recordings were obtained from both sites for at least 40 min following the initial recovery period. Extracellular field excitatory postsynaptic potentials (fEPSPs) were estimated by linear regression over 400 μs along the maximal initial slope (mV/ms) of the test pulses consisting of 100 μs of constant, biphasic current. The stimulus intensity was set to evoke a 1/2 maximal fEPSP slope, based on a stimulus/response curve for each experiment, and was then held constant for the entire experiment. The stimulation data acquisition protocols were administered using custom designed Igor software (WaveMetrics, Lake Oswego, OR). Then, TBS (8 trains of 10 bursts at 5 Hz of 4 pulses at 100 Hz delivered 30 s apart over a total of 3.5 min, Fig. 1b) was administered to one of the two stimulating electrodes. Following TBS, test pulse stimulations resumed, alternating between the control and LTP sites once every 2 min at a 30 s interval between electrodes. Physiological responses were monitored for 5 min (Fig. 1c), 30 min (Fig. 1d), or 120 min (Fig. 1e) after the first train of TBS and then rapidly fixed as described below. The stimulating electrode assigned to deliver TBS was counter-balanced for side of the recording electrode (towards CA3 or subiculum) within times and across experiments.

Tissue Preparation and Processing for 3DEM

Within a few seconds of the end of the experiment, electrodes were removed and each slice was transferred still on its net to 5 ml of mixed aldehydes (6% glutaraldehyde, 2% paraformaldehyde in 100 mM cacodylate buffer with 2 mM $CaCl_2$, and 4 mM $MgSO_4$) and microwaved at full power (700W microwave oven) for 10 s to enhance penetration of the fixative through the depth of the slice with a final temperature of <35°C (Jensen and Harris, 1989). Slices were left overnight in the same fixative and then rinsed with 0.1*M* cacodylate buffer (3× for 10 min), embedded in 7% low melting temperature agarose and trimmed to the region of interest. They were then mounted in agarose and vibrasliced at 70 μm (Leica VT 1000S, Leica, Nusslock, Germany). The vibraslices were placed into a 24-well tissue culture dish (to keep track of position relative to area CA3) and viewed under a dissecting microscope (to determine which vibraslices contained the ~50–100 μm indentations from the two stimulating electrodes).

The two reference and four adjacent vibraslices, two on either side of each stimulating electrode indentation, were processed for 3DEM (Harris et al., 2006; Kuwajima et al., 2013a). First, they were immersed in 1% osmium and 1.5% potassium ferrocyanide in 0.1M cacodylate buffer for 10 min, rinsed in buffer (5×), immersed in 1% osmium and microwaved (1 min on, 1 min off, 1 min on), cooled to 20°C, microwaved again (1 min on, 1 min off, 1 min on), and rinsed in buffer (5× for 2 min) and then water (2×). Next, they were immersed in ascending concentrations of ethanol (50, 70, 90, and 100%) containing 1–1.5% uranyl acetate and microwaved for 40 s after each transfer. Finally, they were quickly rinsed in acetone or propylene oxide (PO) at room temperature, immersed overnight in a 50:50 mixture of acetone or PO:LX112, and then embedded in coffin molds in LX112 and cured for 48 h at 60°C in an oven (Harris et al., 2006).

A small trapezoid was trimmed in the middle of stratum radiatum and 120–150 μm beneath the air surface. From this trapezoid, 150–200 serial sections were cut and mounted on Pioloform-coated slot grids (Synaptek, Ted Pella). Ultrathin sections were counterstained with saturated aqueous uranyl acetate, followed by Reynolds lead citrate (Reynolds, 1963) for 5 min. Sections were photographed, blind as to condition, on a JEOL 1230 electron microscope with a Gatan digital camera at 5,000× magnification along with a diffraction grating replica for later calibration (0.463 μm cross line EMS Catalog #80051 Hatfield, PA or Ernest Fullam, Latham, NY). All image series were assigned distinct 5-letter codes to mask the experimental condition.

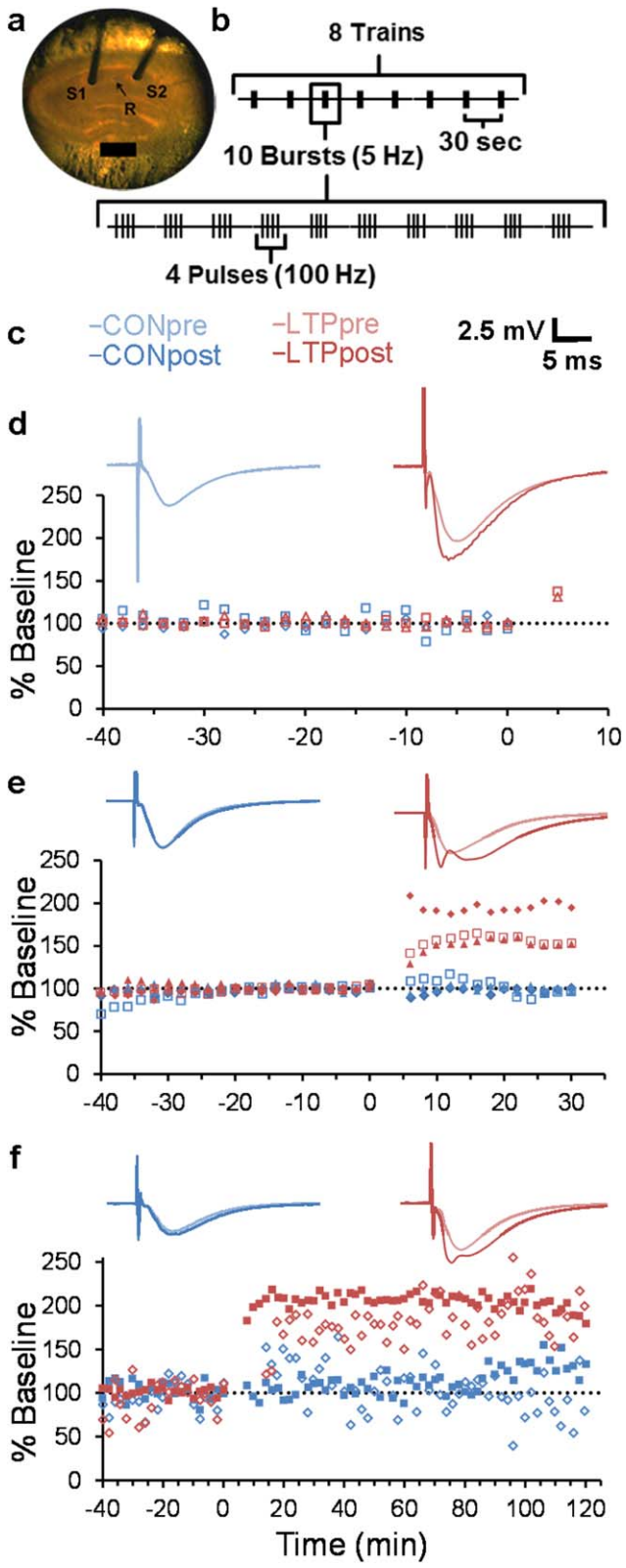

FIGURE 1. Within-slice design and physiological outcomes. (a) Representative acute slice from P15 rat hippocampus illustrating the recording electrode (R, arrow) positioned in the middle of s. radiatum and two bipolar stimulating electrodes (S1 and S2) placed with a separation of ~300–400 μm on either side of the recording electrode (scale = 500 μm). (b) TBS protocol used to produce LTP at S1 or S2, alternating between experiments. (c) Color coding and scale bar (2.5 mV by 5 ms) is for the representative waveforms from CON (blue) and LTP (red) sites above each of the graphs in (d–e). Each representative waveform is an average of responses to each stimulating electrode obtained for the last 20 min prior to the delivery of TBS at time 0 (light blue or light red) and for the entire recording period following TBS (dark blue or dark red). Points on each graph are expressed as a percentage of the average baseline slope obtained for 20 min prior to TBS that was delivered at time 0. The responses were recorded for (d) 5 min ($n = 2$ slices), (e) 30 min ($n = 3$ slices), or (f) 120 min ($n = 2$ slices) after the first TBS train and then fixed and processed for 3DEM as described in "Methods". Since it takes 3.5 min to complete all 8 trains of TBS in this paradigm, only one pulse could be obtained for each experiment at a 30 s interval, in order to demonstrate potentiation, and then fix the slice within 5 min after the first train of TBS. The post-TBS waveforms in (e) and (f) show a positive deflection at ~3–4 ms reflecting the synchronous firing of the pyramidal cells with this strong level of potentiation. [Color figure can be viewed in the online issue, which is available at wileyonlinelibrary.com.]

Perfusion Fixation Procedure

Two P15 male Long-Evans rats (R88 and R89) were deeply anesthetized with pentobarbital (80 mg/kg) and perfused through the heart with fixative (2.5% glutaraldehyde, 2% paraformaldehyde in 100 mM cacodylate buffer with 2 mM $CaCl_2$, and 4 mM $MgSO_4$). Whole brains were removed after at least 1 h and postfixed overnight in the same fixative, but with 6% glutaraldehyde to match the slice postfixation condition. Brains were rinsed in buffer and cut into 400 μm slabs and processed for 3DEM as described above.

Three-Dimensional Reconstructions

Electron micrographs were aligned, and dendrites, spines, and synapses were reconstructed using the Reconstruct software [freely available at http://www.synapseweb.clm.utexas.edu (Fiala and Harris, 2001b; Fiala and Harris, 2002; Fiala, 2005; Harris et al., 2015)]. Pixel size was calibrated in reconstruct from several 10 μm lines on the calibration grid. Section thickness was set at 45 nm on the ultramicrotome. However, the actual section thickness can be influenced by uncontrollable parameters (e.g., subtle variations in knife edge, room temperature, air

TABLE 1.

Sample Sizes (counts) of Dendrites, Synapses, and Potential Synaptic Precursors Under Each Condition

	Perfused		5 min		30 min		120 min	
Condition	R88	R89	CON	LTP	CON	LTP	CON	LTP
Section thickness (nm)	43	53	53–54	53–60	46–50	48–50	56–63	46–55
# Dendrites	9	8	19	20	23	28	24	46–55
Avg length (μm) (±SD)	4.3 (1.2)	41 (1.1)	4.1 (0.5)	3.8 (0.7)	41 (1.0)	43 (1.0)	40 (0.6)	3.5 (0.4)
Synaptic structures								
sp (single)	32	32	98	85	128	195	72	112
sp (multi)	11	15	33	27	66	55	6	33
sp (br)	2	4	22	12	14	49	2	21
sp (sym)	6	0	1	0	1	0	0	1
sh (sym)	4	2	7	3	9	8	3	5
sh (asym)	9	8	14	14	17	5	10	18
Potential synaptic precursors								
ss (sh)	3	3	0	1	4	1	2	4
ss (single)	1	1	0	3	5	7	2	3
ss (multi)	2	2	1	1	2	2	0	0
ss (filo)	5	0	3	0	3	4	4	1
filo (sh)	8	1	9	10	8	15	20	18
filo (sp)	9	1	6	11	4	6	8	4

The analyzed dendritic segments spanned at least 100 serial sections. There were no statistically significant effects of segment length for any of the results reported in this paper. Abbreviations: Avg—average; Sp—spine; Sh—shaft; ss—surface specialization; filo—filopodium; single—one synapse; multi—multisynaptic; br—branched; sym—symmetric; asym—asymmetric. By definition, all dendritic spines had at least one asymmetric synapse.

currents, etc.), all of which we have established parameters to minimize (Harris et al., 2006). As a further control, section thickness was determined by measuring mitochondrial diameters and counting the number of sections they traversed as described for the cylindrical diameters method (Fiala and Harris, 2001a). The calculated section thicknesses ranged from 44 to 63 nm across all conditions (Table 1). This variation in section thickness had no effect on the ability to detect spine origins. In addition, section thickness was included as a parameter, and found not to have any influence on the relative or absolute statistical outcomes. All of the data values are presented in terms of the calculated section thicknesses because they are more accurate than the ultramicrotome setting.

Synapse areal reconstructions

Asymmetric, excitatory synapses (with a thickened postsynaptic density (PSD) and round presynaptic vesicles) were distinguished from symmetric, presumably inhibitory synapses (with thin PSDs and flattened, irregular presynaptic vesicles). Cross-sectioned synapse areas were calculated by multiplying their traced lengths by section thickness and summing across the sections they spanned. Synapses that were cut parallel to the sectioning plane (i.e., en face) were measured by the area on the single section in which they appeared. Obliquely sectioned PSDs often spanned multiple sections and had cross-sectioned, en face, and obliquely sectioned portions. Total synaptic input was determined by summing the areas of all excitatory synapses and dividing by the dendritic segment length (ΣPSD area/μm).

Z-trace lengths

The *Z* trace tool is described in the Reconstruct manual and was used to compute the shortest length along a trajectory through the center of the object being measured. In practice, to measure dendritic segment length the cursor was placed in the center of the dendritic shaft and then the user paged through the series, only adjusting the center point as the dendrite's trajectory turned and the cursor's position moved outside the dendritic profile. Similarly, the *z* lengths were measured for spine dimensions. Then, a 3D reconstruction was viewed from all angles to ensure that the *z* trace followed the actual internal trajectory of the object (dendritic shaft, spine neck, spine head, or spine length). *Z* traces were adjusted and reviewed in 3D as needed.

Sample dendrites

Prior work showed a positive correlation between dendrite cross-sectional area and spine density with microtubule (MT) number in the hippocampus (Fiala et al., 2003; Harris et al., 2007; Bowden et al., 2008). To avoid this bias, only cross-sectioned dendritic segments containing 5–25 MTs were selected for analysis, blind as to condition. Some of the reconstructed segments were substantially longer than others; hence their lengths were shortened to a common average length (4.00 ± 0.07 μm) and were analyzed separately. We used unbiased stereological lengths to estimate the longest length available per dendrite in

each series, without double counting spines (Fiala and Harris, 2001b). The number of dendritic segments available in each image series that met these criteria ranged from 17 (perfused) to 28 (30 min LTP) across conditions (Table 1). This variation in dendritic segments was tested and shown to have no significant effect on the statistical analyses.

Statistical Analyses

The statistical package STATISTICA (StatSoft, Tulsa, OK) was used for all analyses. There were seven groups: perfusion-fixed *in vivo* (PF), and control (CON) and LTP conditions at 5, 30, and 120 min following TBS. At each time point, the CON and LTP groups were evaluated separately relative to the PF condition to determine effects of time *in vitro*, and then relative to each other to establish the LTP effects. Separate hierarchical nested ANOVAs (hnANOVAs) were run with dendrite nested in condition (CON vs. LTP vs. PF) for each measure and at each time point. Since spine and synapse dimensions were highly skewed, all hnANOVAs were performed on natural log transforms of the measured values. Since all density (#/μm) data involved one measurement per dendrite, hnANOVAs were unnecessary; therefore, separate condition (CON vs. LTP vs. PF) one-way ANOVAs were performed at each time point. Results of the hnANOVAs and one-way ANOVAs are reported as ($F_{(df\ \text{condition},\ df\ \text{observations})} = F$ value, P value) where df is degrees of freedom. All comparisons were then tested with *post hoc* Tukey analyses to determine which groups within a time point were significantly different from one another.

Data in bar graphs are plotted as the observed mean ± SEM from the untransformed data. Significant P values determined by the *post hoc* Tukey's analyses of log-transformed data are indicated by asterisks above the bars or as specific values in the figure legends. None of the reported findings were carried by individual dendrites in any condition or time point. Individual raw data points are also plotted in graphs to illustrate correlations analyzed with analyses of covariance (ANCOVA) where appropriate. The specific statistical results are indicated in the associated figure legends, and significance was set at $P < 0.05$.

RESULTS

Only slices with input-specific LTP (Fig. 1) and excellent tissue quality (Fig. 2) were used for 3DEM analyses. Synapses and dendritic spines were characterized by a variety of geometrical and synaptic characteristics [Table 1, Supporting Information Figure (S)1]. Most dendritic spines had a single asymmetric synapse with a thickened PSD (Fig. 2a–e,g). The rare multisynaptic spines had 2–3 PSDs (Fig. 2f). Each branch of a branched dendritic spine had a separate synapse (Fig. 2h). Synapses on single synaptic spines accounted for most of the contacts, followed by multisynaptic and branched spines (Supporting Information Fig. S1). These three categories of dendritic spines were analyzed separately from excitatory and inhibitory shaft synapses, surface specializations, and filopodia. To determine whether spine dimensions were altered during LTP or control stimulation relative to PF hippocampus, we used 3DEM to measure features (neck diameter, total spine length, and head diameter) that are critical to the biophysical and biochemical functions of dendritic spines (Fig. 2a, inset).

Late Addition of Small Dendritic Spines Had Little or No Effect on Magnitude of LTP

Changes in the density of spines (Fig. 3a) required time to manifest after TBS, as there were no changes at 5 min either at the CON or LTP sites relative to PF hippocampus (Fig. 3b). By 30 min, there was a higher spine density with LTP relative to PF hippocampus (Fig. 3b). By 120 min, the spine density remained elevated during LTP, but the control stimulation alone reduced spine density relative to PF (Fig. 3b). These effects were carried primarily by single dendritic spines (Fig. 3c), although branched spines (Fig. 3d), and multisynaptic spines (Fig. 3e) showed smaller, but statistically significant increases at 120 min in the LTP condition.

Biophysical properties of individual dendritic spines can be affected by their lengths and diameters. As such, the high neck resistance of dendritic spines can serve to passively amplify local depolarization at the synapse (Harnett et al., 2012). Recent models suggest that spines with constricted necks could also serve to equalize the strength of synaptic input throughout the dendritic arbor (Gulledge et al., 2012). Furthermore, sufficient shortening or widening of spine necks could facilitate potentiation. Here, we tested for changes in spine dimensions following induction of LTP with TBS versus time-matched control stimulation at different synapses of the same slices (Figs. 4 and Supporting Information S2).

Since the magnitude of potentiation did not change between 30 and 120 min (Fig. 1d, e), the sustained increase in synapse density raised the question of whether the added spines might be small and effectively silent. Average spine neck diameters were unaffected by LTP across time, although there was a subtle decrease at 30 min relative to PF that was gone by 120 min (Fig. 4a). Spines were longer (Fig. 4b) and had wider heads (Fig. 4c) at 5 min after induction of LTP, but these average changes did not last. Average spine head diameters were larger under CON than LTP conditions at 120 min, but neither differed significantly from PF hippocampus (Fig. 4c).

Analysis of spine densities by dimension at 120 min revealed that most of the added spines in the LTP condition were smaller than those in the time-matched controls, having thin necks (Fig. 4d), long lengths (Fig. 4e), and thin heads (Fig. 4f). These changes in the relative densities of spines with different dimensions were not observed at 5 or 30 min (Supporting Information Fig. S2).

Spine dimensions were highly variable among spines in all conditions. Nevertheless, longer spines were found to have thinner necks at all times and conditions (Supporting Information Fig. S3a–c). At 5 min, the relationship between neck diameter and length did not change after the induction of LTP

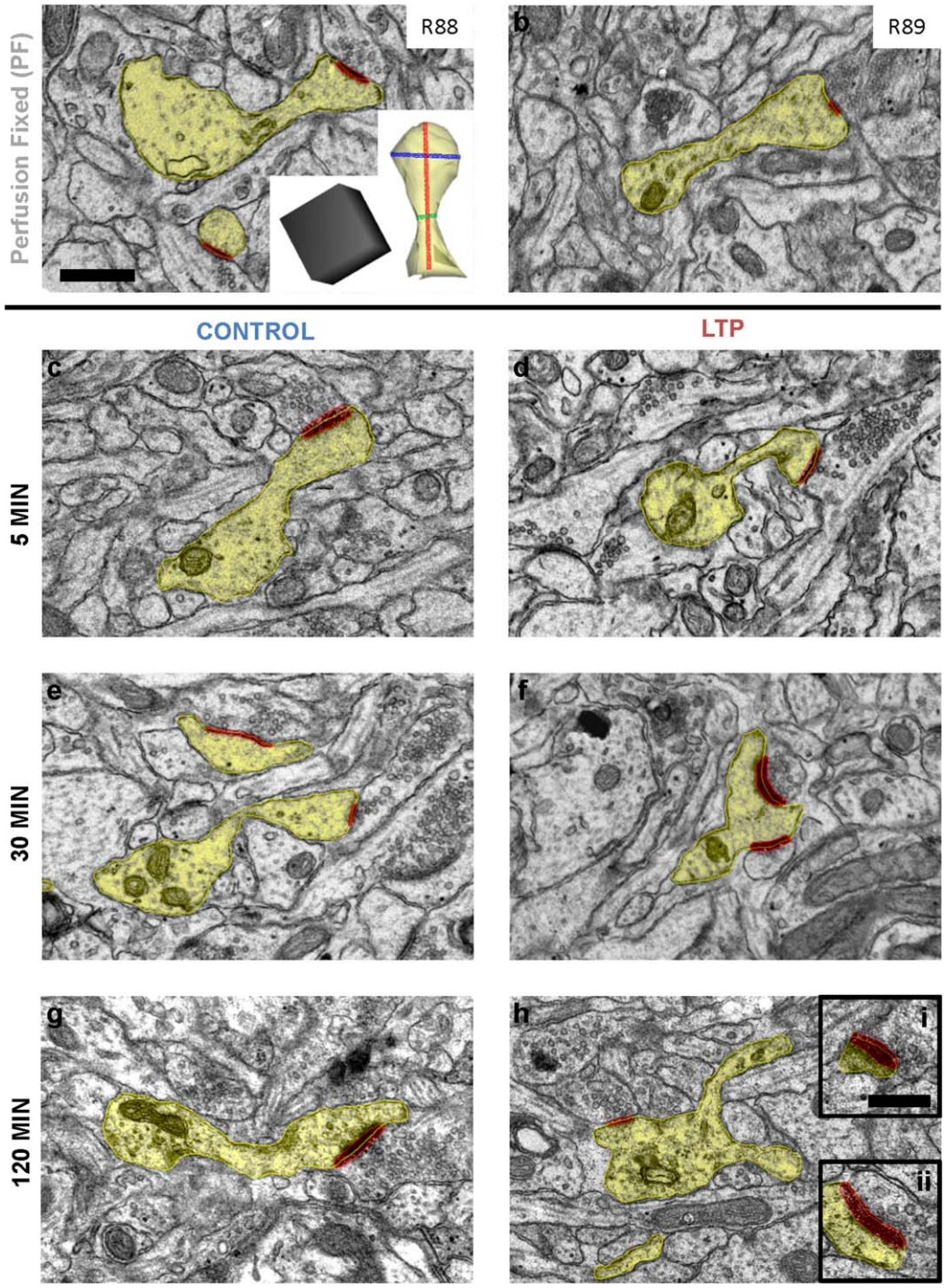

FIGURE 2. Representative electron micrographs from perfusion-fixed hippocampus and control and LTP conditions at each time following TBS. High quality of tissue preservation in perfused-fixed hippocampus of (a) R88 and (b) R89 is comparable to all of the acute slices in the 5 min (c) CON and (d) LTP conditions; the 30 min (e) CON and (f) LTP conditions; and the 120 min (g) CON and (h) LTP conditions. Portions of sample dendrites and spines (yellow) in each EM are illustrated with example asymmetric, presumed excitatory (red) synapses. The reconstructed spine inset in (a) illustrates representative *z* traces in 3DEM of the total spine length (red) and the head (blue) and neck (green) diameters. The branched spine in 2 h has a wide base containing SER and polyribosomes. Scale bar in (a) is 500 nm for (a–h), and the 3D cube = 500 nm per side. [Color figure can be viewed in the online issue, which is available at wileyonlinelibrary.com.]

(Fig. 4g). However, head diameter was significantly wider across all neck diameters at 5 min after induction of LTP (Fig. 4h) and among the shortest spines (Fig. 4i). Interestingly, more of the shorter spines had thinner necks at 120 min after the induction of LTP versus the time-matched controls (Fig. 4j). The head diameters were significantly narrower across the range

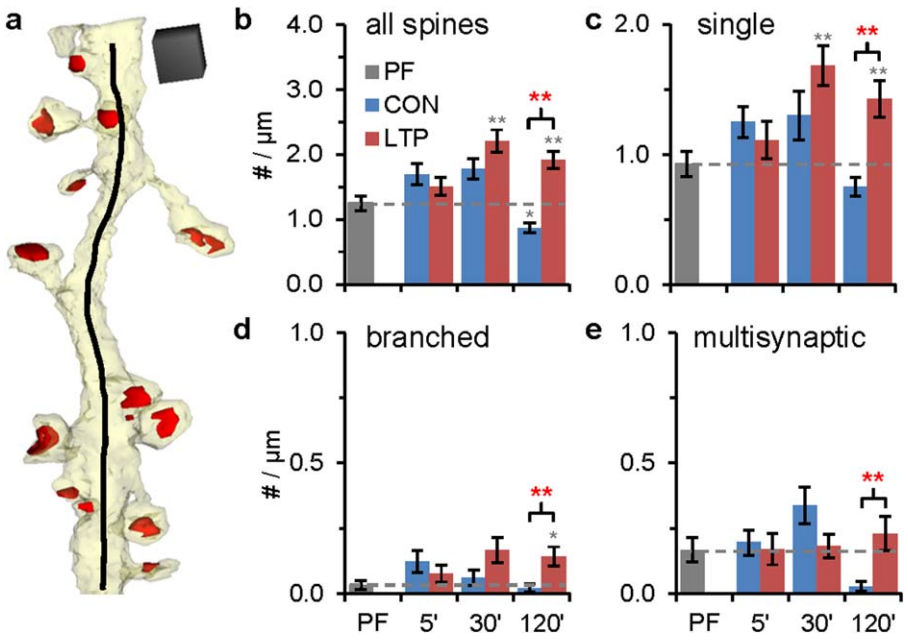

FIGURE 3. Changes in spine density during LTP. (a) Representative 3D reconstruction of a dendrite (from 30 min LTP condition) illustrating the *z* length (black) used to calculate spine or synapse (red) densities. Scale cube is 500 nm per side. (b–e) Statistical findings from ANOVAs compared CON, LTP, and PF within time points and are presented as ($F_{(df\ condition,\ df\ observations)} = F$ value, P value). Significant *post hoc* Tukey's results have stars above columns (*$P<0.05$, **$P<0.01$, ***$P<0.0001$) showing differences from PF with gray stars, and differences between LTP and CON in red stars and top brackets (see "Methods"). (b) Changes in total spine density at 30 min ($F_{(2,65)} = 8.28$, $P<0.001$) and 120 min ($F_{(2,60)} = 26.45$, $P<0.0001$). (c) Changes in single spine density at 30 min ($F_{(2,65)} = 5.30$, $P = 0.007$) and 120 min ($F_{(2,60)} = 11.41$, $P<0.0001$). (d) Change in branched spine density at 120 min ($F_{(2,60)} = 7.27$, $P<0.001$). (e) Change in multisynaptic spine density at 120 min ($F_{(2,60)} = 5.34$, $P = 0.007$). [Color figure can be viewed in the online issue, which is available at wileyonlinelibrary.com.]

of spine neck diameters by 120 min after the induction of LTP versus the time-matched controls (Fig. 4k), but this relationship was uncorrelated at 5 and 30 min (Supporting Information Fig. S3g–i). Furthermore, at 120 min, the spines in the LTP condition had narrower head diameters across all spine lengths than the time-matched controls (Fig. 4l).

Overall these findings suggest that spine necks did not shorten and widen following induction of LTP at P15. In fact, there were no significant changes in neck diameter with condition or across time. Instead, the spine heads initially swelled and spines elongated on average by 5 min after the induction of LTP with TBS. Later, the dendritic spines that were added in the LTP condition had similarly thin necks as the CON spines and were of the smallest dimensions. As such, they would not have made significant contributions to the potentiated response.

Added Spines Had Small Synapses During LTP

We determined the size of synapses as a proxy for synaptic strength to test the hypothesis that the sustained increase in spine density during LTP involved addition of functionally less effective or silent synapses. The surface apposition area of each PSD was measured for every spine with a single synapse and for each synapse on a branched or multisynaptic dendritic spine (Fig. 5a–c). The frequency distributions of spines were not uniform, either in number or size; hence, computing the overall averages in PSD area was not meaningful. Instead, we analyzed for changes in density, per length of dendrite, of PSDs of different sizes (Fig. 5d–f). At 5 min after the induction of LTP, a couple large synapses occurred that were not found in the CON or PF conditions; otherwise, the differences were not significant among conditions at this time (Fig. 5d). By 30 min, dendrites from both CON and LTP conditions had higher densities of the smallest PSDs relative to PF (Fig. 5e). At 120 min, the density of the smallest PSDs decreased in the CON group relative to PF, but increased with LTP relative to both the CON and PF conditions, while the density of larger synapses was unchanged (Fig. 5f). That only small synapses were added suggests they could be functionally ineffective, which would explain why potentiation was not further enhanced at 30 or 120 min after TBS.

Next, we determined whether the new small synapses were also on the small dendritic spines. PSD area and spine head diameter had a strong positive correlation across all times and conditions (Fig. 5g–i), and their covariance increased slightly at 5 min after LTP induction, consistent with the transient increase in head diameter and total length (compare Fig. 4b,c). PSD areas were also well-correlated with spine neck diameter such that spines with larger PSDs had wider necks, providing for greater charge transfer and efficacy at larger synapses (Fig. 5j–l). For this analysis, we excluded spines with equal neck and head diameters as this shape would not have an impact on

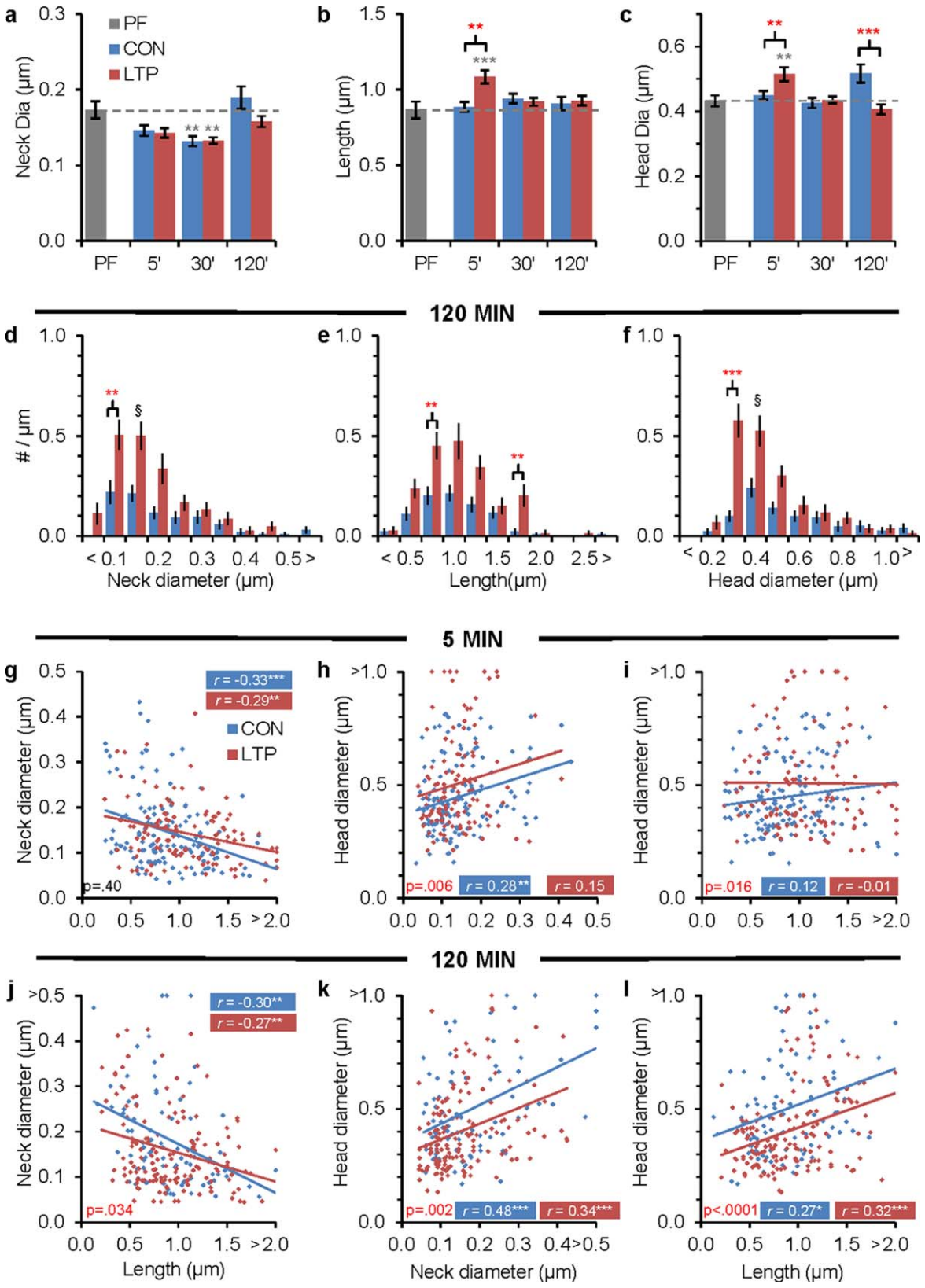
a
Neck Dia (µm)
PF
CON
LTP
PF 5' 30' 120'
b
Length (µm)
c
Head Dia (µm)
120 MIN
d
/ µm
Neck diameter (µm)
e
Length(µm)
f
Head diameter (µm)
5 MIN
g
Neck diameter (µm)
r = -0.33***
r = -0.29**
p=.40
h
Head diameter (µm)
p=.006
r = 0.28**
r = 0.15
i
p=.016
r = 0.12
r = -0.01
120 MIN
j
r = -0.30**
r = -0.27**
p=.034
Length (µm)
k
p=.002
r = 0.48***
r = 0.34***
Neck diameter (µm)
l
p<.0001
r = 0.27*
r = 0.32***

FIGURE 4.

charge transfer without the neck constriction. At both 30 and 120 min, PSD areas were smaller across the full range of spine neck diameters (Fig. 5k,i, respectively).

Finally, we assessed whether there was a change in the distribution or size of macular (Fig. 5a) versus perforated (Fig. 5b) synapses. Over all asymmetric synapses, 92% were macular and 8% were perforated (Supporting Information Fig. S4a, Supporting Information Tables S1, S2). For the few synapses with PSD areas greater than 0.2 μm^2 (total 27 for all conditions), 22% were macular, and 78% were perforated (Supporting Information Fig. S4b and Table S3). There was a small increase in the density of perforated synapses in the 30 min LTP condition relative to PF and CON ($F_{(2,65)} = 5.70$, $P = 0.005$), but this effect was not present at 5 min and was not sustained at 120 min. In addition, there were no significant differences in the dimensions of the perforated PSD areas across times or conditions.

These findings are consistent with the unchanged level of potentiation across time following TBS. They support the hypothesis that induction of LTP causes a rapid strengthening of synapses by 5 min. Then new synapses added by 30 min and sustained for at least 120 min by LTP, or subsequently lost during test pulse stimulation, were small, weak, or silent synapses.

Spine Branching was not a Result of Synapse Splitting During LTP

To test whether branched or new spines arose from the splitting of pre-existing spine synapses, we followed branched spine heads to determine if they shared the same presynaptic partners, a necessary intermediate state of splitting (Sorra et al., 1998; Fiala et al., 2002a). Each spine branch was followed through serial sections to identify their presynaptic partners. The spine branches shared the same presynaptic axon in only one case out of the 57 branched spines, with a total of 111 branches across all conditions. Thus, the addition of single or branched spines was not accounted for by synapse splitting.

Effects of LTP on Asymmetric Shaft Synapses

In addition to spinogenesis there is also a small burst of shaft synaptogenesis during the second postnatal week that might support new spine formation (Harris, 1999). To test this hypothesis, we computed the density of asymmetric shaft synapses across conditions and time *in vitro*. Asymmetric shaft synapses were identified by the presence of a thickened PSD on the dendritic shaft (Fig. 6a,b). The presynaptic vesicles were characteristically round and the axonal boutons were similar to those synapsing on dendritic spine heads in the same field. Only ~45% of the sampled dendrite segments had asymmetric shaft synapses, and their frequency was unchanged with LTP, except for a transient decrease relative to CON and PF at 30 min that recovered by 120 min (Fig. 6c). The average PSD area was comparable to the average small spine synapses and not significantly changed across conditions or relative to PF (Fig. 6d). Thus, the transient decrease in the small shaft synapse density suggests that the conversion of shaft synapses into spines could contribute to spine proliferation during LTP. However, to account for the dramatic increase in spine number, there would also need to be a robust increase in the formation and conversion of shaft synapses. We conclude that conversion from shaft synapses to dendritic spines makes only a small contribution to spinogenesis during LTP at P15.

Plasticity of Potential Synaptic Precursors

Other potential sources of new dendritic spines include surface specializations and filopodia [Fig. 7, see also Supporting Information Fig. S1 and (Fiala et al., 1998)]. Surface specializations are characterized by pre- and postsynaptic densities with fewer than three presynaptic vesicles and they occurred on dendritic shafts (Fig. 7a), filopodia (Fig. 7b), and dendritic spines that also had an excitatory synapse (Fig. 7c). Nonsynaptic filopodia (Fig. 7d) occasionally emerged from the dendritic shaft (Fig. 7e) or from spine heads (Fig. 7f), but neither of these potential precursor sites changed significantly in frequency between the PF, CON, nor LTP conditions (Fig. 7e, f). Similarly, changes in the relative proportions of surface

FIGURE 4. Changes in spine dimensions during LTP. (a) Average spine neck diameter decreased transiently at 30 min in both CON and LTP conditions relative to PF ($F_{(2,467)} = 7.66$, $P < 0.001$). (b) Average spine length increased transiently at 5 min during LTP vs. CON and PF conditions ($F_{(2,\ 313)} = 11.13$, $P < 0.0001$). (c) Average head diameter increased transiently at 5 min during LTP vs. CON and PF conditions ($F_{(2,313)} = 6.14$, $P = 0.002$) and decreased at 120 min in LTP versus CON, but not PF, conditions ($F_{(2,299)} = 8.25$, $P < 0.001$). At 120 min a higher density of spines (#/μm) occurred in the LTP vs. CON: (d) for thin neck diameters (0.1–0.2 μm, $F_{(1,\ 42)} = 11.33$, $P = 0.002$), (e) for long lengths (0.75–1.0 μm, $F_{(1,42)} = 9.25$, $P = 0.004$; and 1.75–2.0 μm ($F_{(1,\ 42)} = 10.02$, $P = 0.003$)), and (f) for thin head diameters (0.3–0.35 μm, $F_{(1,42)} = 30.53$, $P < 0.0001$). There were no effects of experiment unless otherwise noted ($—the LTP effect was negated because there was a significant condition × experiment interaction). At 5 min after the induction of LTP: (g) there was no change in spine neck versus length ($F_{(1,\ 245)} = 0.72$), (h) spine heads were larger across all neck diameters ($F_{(1,245)} = 7.66$) and (i) spine heads were larger across the shorter lengths ($F_{(1,245)} = 5.85$). At 120 min after induction of LTP: (j) short spines had thinner necks ($F_{(1,231)} = 4.56$), (k) heads were narrower across spines of all neck dimensions ($F_{(1,\ 231)} = 9.79$). (l) Heads were narrower across all spine lengths with LTP ($F_{(1,231)} = 16.37$). (a–c) Statistical findings are hnANOVAs and (d–f) ANOVAs with *post hoc* Tukey's results, presented as in Figure 3. (g–l) Color-coded correlations show Pearson's r with stars for $^{*}P < 0.05$, $^{**}P < 0.01$, $^{***}P < 0.0001$. ANCOVA results show actual P values (red if significance is $P < 0.05$) at base of each graph; see Supporting Information Figures S2 and S3 for additional density by dimensional analyses at all of the time points. [Color figure can be viewed in the online issue, which is available at wileyonlinelibrary.com.]

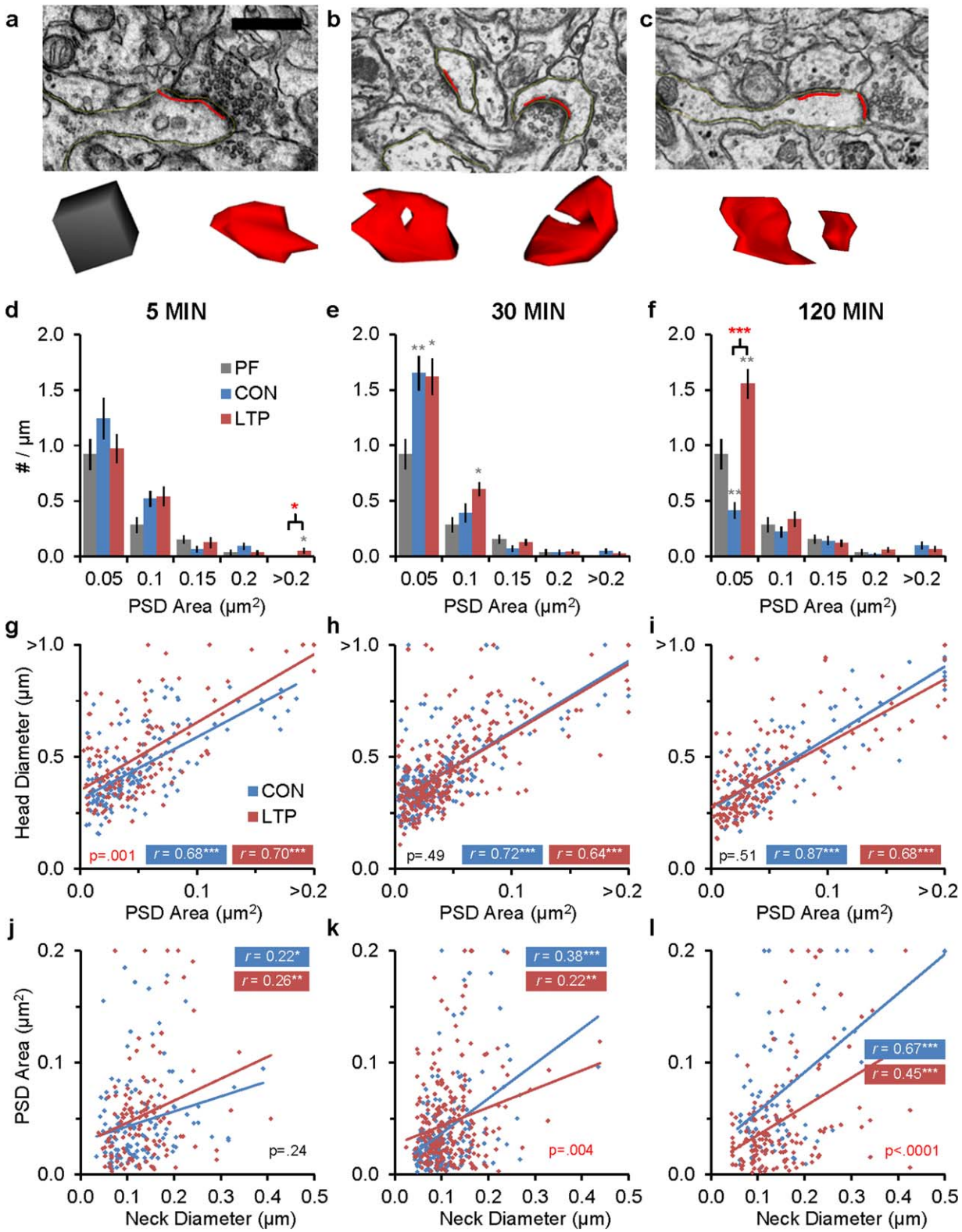

FIGURE 5. Effects of LTP on synapse sizes. (a) Representative EMs and 3Ds from synapses on a single synapse spine in the LTP condition at 5 min, (b) a branched spine in the LTP condition at 30 min, and (c) a multisynaptic spine in the CON condition at 5 min. Scale bar in (a) is 500 nm, and 3D cube = 250 nm per side. (d–f) Density of all spines (#/µm) binned for PSD area: (d) at 5 min, for areas >0.20 µm^2 ($F_{(2,\ 53)} = 4.19$, $P = 0.020$), (e) at 30 min, for PSD areas <0.05 µm^2 ($F_{(2,\ 65)} = 5.71$, $P = 0.005$) and <0.01 µm^2 ($F_{(2,65)} = 5.04$, $P = 0.009$), and (f) at 120 min for PSD areas <0.05 µm^2 ($F_{(2,\ 60)} = 27.68$, $P < 0.0001$). (g–i) Scatterplots illustrate relationships between spine head diameter vs. PSD area: (g) at 5 min ($F_{(1,277)} = 10.59$), (h) at 30 min ($F_{(1,490)} = 0.49$), and (i) at 120 min ($F_{(1,250)} = 0.44$). (j–l) Scatterplots illustrate relationships between PSD area vs. spine neck diameter: (j) at 5 min ($F_{(1,241)} = 1.37$), (h) at 30 min (due to nonparallel slopes, a hnANOVA was performed [$F_{(1,387)} = 8.20$, $P = 0.0004$)], and (i) at 120 min post-TBS ($F_{(1,250)} = 0.44$). (statistical findings are presented as hnANOVAs and *post hoc* Tukey's results in (d–f, k) as in Figure 3 or as correlations and ANCOVAs (g–l) as in Figure. 4. [Color figure can be viewed in the online issue, which is available at wileyonlinelibrary.com.]

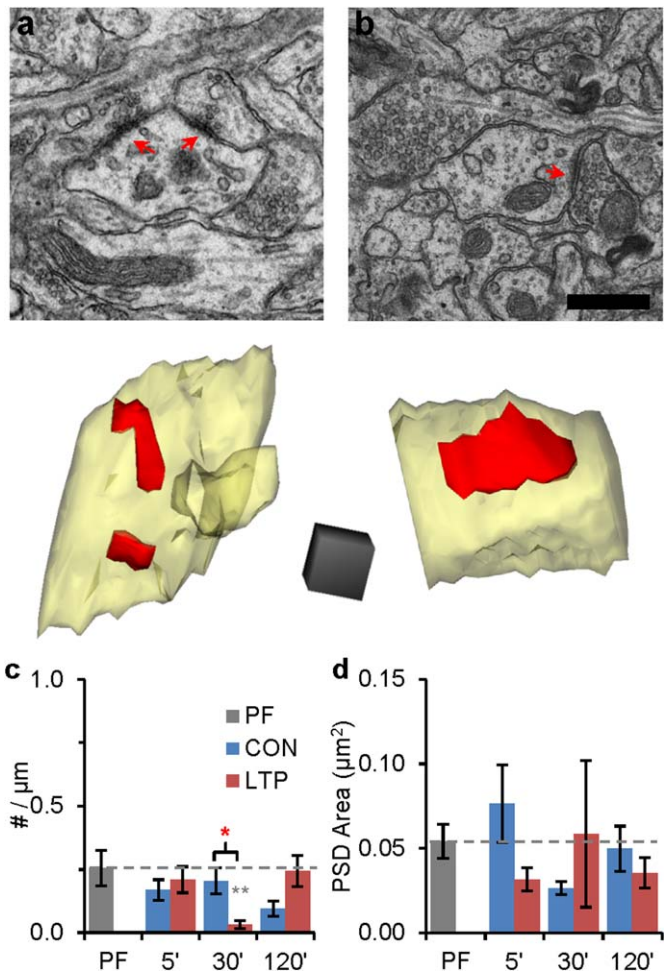

FIGURE 6. Effects of LTP on asymmetric shaft synapses. Representative EMs and 3Ds of asymmetric shaft synapses in (a) CON at 30 min after TBS and (b) LTP conditions at 120 min after TBS. Scale bar is 500 nm and 3D cube is 250 nm per side. (c) The density of asymmetric shaft synapses increased at 30 min ($F_{(2, 65)} = 7.39$, $P = 0.001$), but this increase was not sustained at 120 min ($F_{(2,60)} = 2.91$, $P = 0.06$). (d) Changes in average PSD areas per unit length were not significant [statistical findings are presented as one-way ANOVA with ($F_{(df\ condition,\ df\ observations)} = F$ value, P value) for (c) and hnANOVAs for (d). *Post hoc* Tukey's results have stars above columns as in Fig. 3)]. [Color figure can be viewed in the online issue, which is available at wileyonlinelibrary.com.]

specializations in different locations did not reach statistical significance (Fig. 7g). Overall, there was a decrease in the density of surface specializations in both CON and LTP conditions relative to PF, an effect that was most pronounced at 5 min (Fig. 7h). These subtle changes in surface specializations and filopodia may contribute to, but do not account for, new spine and synapse formation and preservation during LTP at P15.

Plasticity of Symmetric Synapses

Symmetric synapses typically are inhibitory and/or neuromodulatory (Kisvarday et al., 1990; Nusser et al., 1996; Somogyi et al., 1996; Harris and Weinberg, 2012) and were positioned on dendritic shafts amongst the origins of dendritic spines (Fig. 8a,b) where they might alter the effects of excitatory input. The density of symmetric synapses was low in all conditions and was further diminished during 120 min of control stimulation relative to PF hippocampus (Fig. 8c). The apparent decreases in their average synaptic area did not reach statistical significance (Fig. 8d). However, the combination of subtle changes in density and synapse area revealed a significant decrease in the summed area of inhibitory synapses in both the CON and LTP conditions by 120 min, relative to PF hippocampus (Fig. 8e). The correlation between summed inhibitory synapse area and total number of inhibitory synapses per dendritic segment length was retained at 120 min (Fig. 8f). Only ~25% of the dendritic segments in our samples had symmetric synapses, hence analyses of longer dendritic segments may be needed to understand their role in LTP. Nevertheless, the findings suggest that a subtle decrease in inhibition from test pulses occurs under both CON and LTP conditions relative to PF in P15 hippocampus.

Effect of Synaptogenesis on Total Synaptic Input per Dendrite during LTP

In adult hippocampal area CA1, small spines recovered to PF levels during control test pulse stimulation, whereas LTP curtailed small spine formation and produced larger synapses. This dramatic structural remodeling was balanced and total excitatory synaptic input, expressed as the summed PSD area per micron length of dendrite, was equal across all conditions in adult hippocampus (Bourne and Harris, 2011; Bell et al., 2014).

Here, we tested whether this structural synaptic scaling occurs in P15 hippocampus following the induction of LTP. Total excitatory synaptic input (ΣPSD area/µm) was evaluated relative to excitatory synapse density (#asym syn/µm) per micron length of dendrite across all conditions (Fig. 9). There was a significant positive correlation between the density of excitatory synapses and summed PSD area in PF R89 (Fig. 9a,b), and under both CON and LTP conditions at 5 min (Fig. 9c,d) and 30 min (Fig. 9e,f). Since P15 is an age of robust synaptogenesis, it is not surprising that the variation amongst PF dendrites was sufficient in R88 that the correlation did not reach significance. By 120 min, the correlation in the CON condition also broke down with the loss of spines during test pulse stimulation, such that the summed areas were equally distributed across the full range of spine densities from ~0.3 to 2 synapses/µm (Fig. 9g,h). In contrast, at 120 min following the induction of LTP with TBS, the increase in spine density that had been sustained since 30 min resulted in a greater summed PSD area (0.11 ± 0.01 µm^2/µm) relative to the control test pulse stimulation in the same slices (0.084 ± 0.01 µm^2/µm) (Fig. 9h). This increase was still less than about 30% of the total summed PSD area (averaging 0.3 ± 0.02 µm^2/µm) found in adult hippocampus (Bourne and Harris, 2011). These findings suggest that when developing dendrites add new spines, structural synaptic scaling is not triggered because the

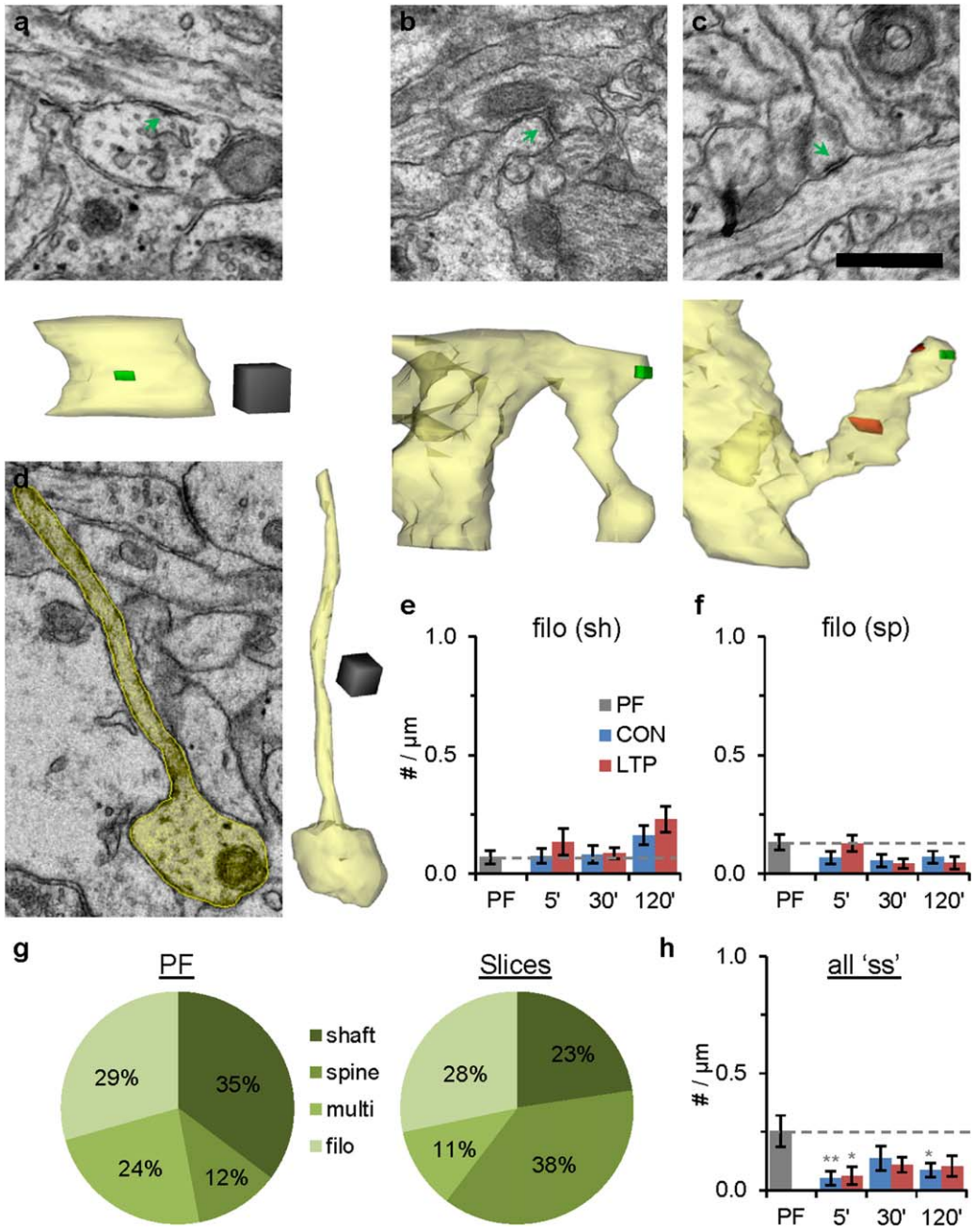

FIGURE 7. No LTP-related changes in the emergence of nonsynaptic surface specializations or filopodia. Representative EMs and 3D reconstructions of surface specializations on (a) the dendrite shaft, (b) nonsynaptic protrusions, (c) a multisynaptic spine. (d) EM and 3D of a filopodia emerging from a dendritic shaft. Scale bar is 500 nm and the 3D cube is 250 nm per side. (e) Density of filopodia emerging from dendritic shaft, and (f) spines with filopodia did not undergo statistically significant changes across conditions or time. (g) Changes in the percentage of all surface specializations at different locations did not reach statistical significance between PF and acute slice conditions ($\chi^2 = 4.91$, $P = 0.18$). (h) There were too few surface specializations to test LTP vs. CON based on location; however, the overall density of surface specializations pooled across locations was greater in PF relative to both 5 min conditions ($F_{(2,\ 53)} = 5.87$, $P = 0.005$) and to the 120 min CON condition ($F_{(2,60)} = 3.63$, $P = 0.03$). [Statistical findings are presented as ANOVAs with ($F_{(df\ \text{condition},\ df\ \text{observations})} = F$ value, P value) for e, f, h, and the *post hoc* Tukey's results have stars above columns as in Fig. 3.]. [Color figure can be viewed in the online issue, which is available at wileyonlinelibrary.com.]

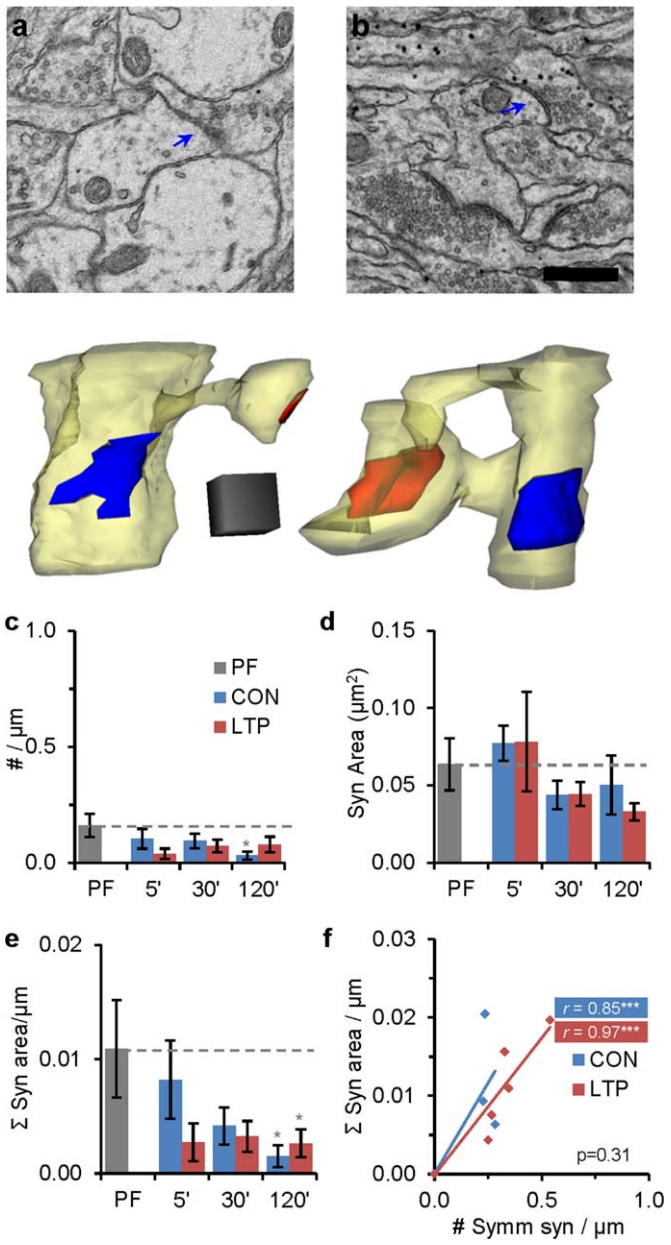

FIGURE 8. Effects of test pulses and TBS on inhibitory synapses. (a, b) Representative EMs and 3D reconstructions of symmetric synapses on dendritic shafts. Scale bar is 500 nm and 3D cube is 250 nm per side. (c) Density of symmetric spine and shaft synapses decreased by 120 min in the CON condition relative to PF ($F_{(2,\ 60)} = 3.69$, $P = 0.03$). (d) Differences in the average synapse area for symmetric shaft synapses did not reach statistical significance across conditions or time. (e) Summed symmetric synaptic input per micron dendrite length decreased significantly for both CON and LTP conditions relative to PF by 120 min ($F_{(2,\ 60)} = 4.86$, $P = 0.01$). (f) Although summed symmetric area per micron of analyzed dendritic length vs. symmetric synapse density were well-correlated, they did not differ significantly across LTP and CON conditions at any time; 120 min is shown here ($F_{(1,\ 43)} = 1.05$, $P = 0.31$). (Statistical findings are presented as ANOVAs for (c), (e) or hnANOVA for (d) as in Figs. 3 and 4.). [Color figure can be viewed in the online issue, which is available at wileyonlinelibrary.com.]

added input can be accommodated along the immature potentiated dendrites.

DISCUSSION

These are the first 3DEM analyses of dendritic spines and synapses following the induction of LTP in the developing hippocampus. They demonstrate a rapid increase, by 5 min after TBS, in spine lengths and head diameters, but not neck diameters. By 30 min, there was a marked increase in the density of spines with small synapses that was sustained for at least 120 min. In contrast, control test pulses resulted in the loss of spines with small synapses. Both the addition of spines following TBS and their loss with test pulse stimulation appear to be silent processes as there was no consistent elevation or decrement in potentiation or control responses, respectively. Interestingly, the addition of small spines following the induction of LTP resulted in an increase in total synaptic area per unit length of dendrite by 120 min. This elevation was still much less than the total synaptic input found along mature dendrites. Thus, unlike adults where structural synaptic scaling is triggered to balance total input along dendrites (Bourne and Harris, 2011; Bell et al., 2014), the immature P15 dendrites were able to accommodate substantial synaptogenesis following the induction of LTP by TBS.

The initial enlargement of spines at 5 min following TBS is consistent with results from glutamate-uncaging and other forms of local activation that rapidly increase spine head size and AMPAR number (Matsuzaki et al., 2004; Park et al., 2004; Kopec et al., 2006; Park et al., 2006; Kopec et al., 2007; Ehrlich et al., 2007; Lee et al., 2009; Meyer et al., 2014). Similarly, the sustained increase in spine density following TBS is consistent with the delayed increase in small dendritic protrusions seen following glutamate-uncaging and local activation of cultured hippocampal neurons (Maletic-Savatic et al., 1999; Engert and Bonhoeffer, 1999; Toni et al., 1999; Tominaga-Yoshino et al., 2008). As with our study, spine necks did not shorten or widen with glutamate-uncaging in acute hippocampal slices from developing mice imaged with super-resolution light microscopy (Takasaki and Sabatini, 2014). In contrast, spine necks became wider and shorter after glutamate-uncaging in organotypic slices that were also imaged with super-resolution light microscopy (Tonnesen et al., 2014). Spine neck widths were all of a comparable range (i.e., 0.05 to 0.34 µm) despite methodological differences between these two studies and the 3DEM results reported here. More research is clearly needed to understand the full impact of diversity in spine neck dimensions on synaptic plasticity.

Our 3DEM analyses revealed no changes in the potential spine precursors, nonsynaptic filopodia or surface specializations. However, the additional spines had smaller heads and synapses than CON spines. The number of excitatory and inhibitory shaft synapses per micron length of dendrite was not

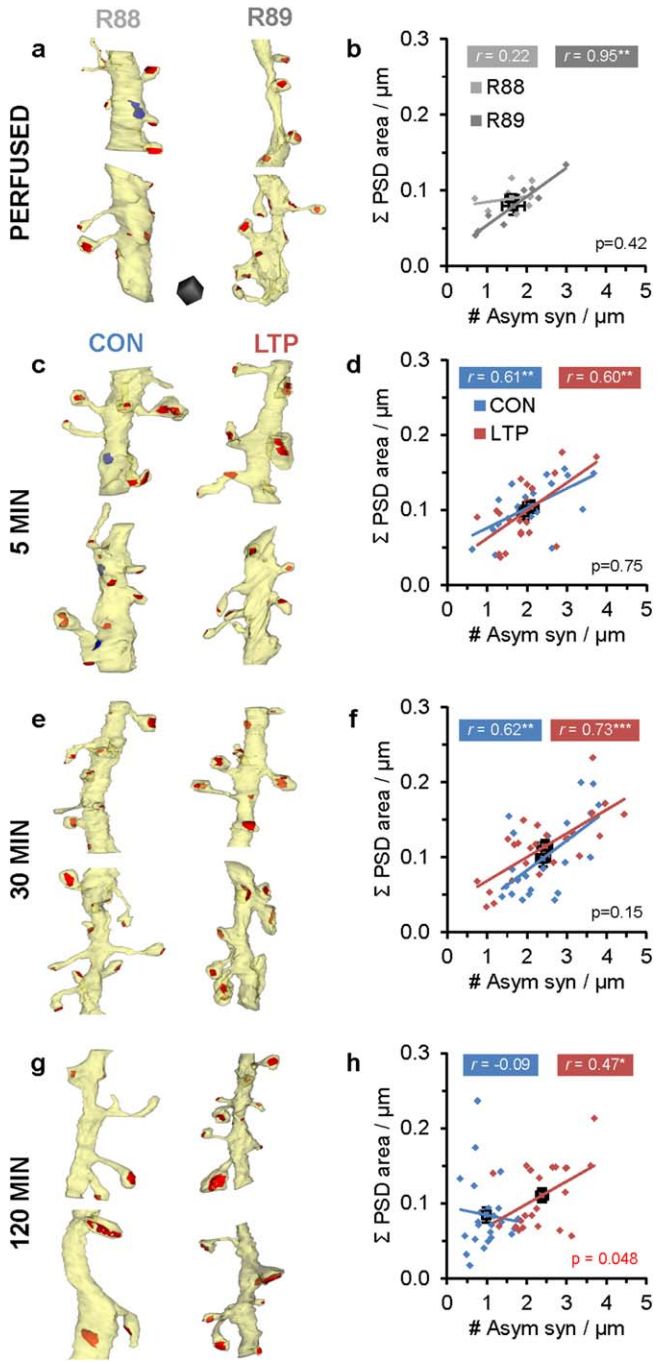

FIGURE 9. Total PSD area per unit length of dendrite compared across conditions within times. (a, b) Perfused animals R88 and R89 ($F_{(1,15)} = 0.69$), and (c, d) at 5 min ($F_{(1,36)} = 0.10$), (e, f) at 30 min ($F_{(1,\ 48)} = 2.12$), and (g, h) at 120 min ($F_{(1,\ 42)} = 4.17$). Means are plotted with error bars for both axes in the center of each scatterplot. Statistical findings are presented as ANCOVAs with *P* values (d, f) or one-way ANOVAs for ΣPSD areas only when the slopes were nonparallel (b, h), and with stars for correlations as in Figure 4. The 3Ds of dendritic segments are from the ~50th percentile (range: 37–57) of asymmetric synapse density (both spine and shaft synapses are included). Asymmetric synapses (red) and symmetric synapses (blue) are illustrated. Scale cube in (a) is 500 nm on a side for all these 3D reconstructions. [Color figure can be viewed in the online issue, which is available at wileyonlinelibrary.com.]

altered following LTP. Thus, both local activation of a single or few spines and co-activation of many synapses with TBS initially enlarges individual synapses and later enhances spine formation in developing hippocampus. In contrast, TBS at multiple synapses in adults causes enlargement of existing synapses at the expense of ongoing spinogenesis (Bourne and Harris, 2011; Bell et al., 2014). Interestingly, strong activation of a single spine along young dendrites in organotypic slice cultures results in the loss of neighboring dendritic spines (Oh et al., 2015). It remains to be determined whether this difference can be explained by dendrites being cultured since birth versus acute slices, where dendrites first grew to their P15 age *in vivo* before slicing. Alternatively, intense activation of a single synapse may trigger different mechanisms from the coordinated activation of multiple inputs.

In previous work from P15 hippocampal slices the density of spines was unchanged at 120 min following the induction of LTP by tetanic stimulation (Ostroff et al., 2002). The present results suggest that the more naturalistic TBS protocol produced new spines that had not been triggered by the weaker tetanic stimulation protocol (2 times at 100 Hz for 1 s at a 20 s interval). In support of this hypothesis, TBS and tetanic stimulation also differ in the onset age of enduring LTP. Whereas tetanic stimulation first produced enduring LTP at P15 (Harris and Teyler, 1984; Harris et al., 1992; Jackson et al., 1993), TBS produced enduring LTP by P12, coincident with the onset age of dendritic spine formation in rat hippocampus (Kirov et al., 2004; Cao and Harris, 2012). Tetanic stimulation and TBS both activate NMDA receptors and elevate postsynaptic calcium via that route. TBS also engages voltage-dependent calcium channels, back-propagating action potentials, and calcium stores, as well as growth factors like BDNF (Staubli and Lynch, 1987; Nguyen and Kandel, 1997; Morgan and Teyler, 2001; Buzsaki, 2002; Raymond and Redman, 2002; Raymond and Redman, 2006). Hence, TBS could enhance postsynaptic Ca^{2+} and stabilize more AMPARs (Isomura and Kato, 1999; Kramar and Lynch, 2003; Yasuda et al., 2003; Abrahamsson et al., 2007, 2008; Yang et al., 2009).

Control test pulse stimulation alone resulted in spine loss by 120 min, relative to PF hippocampus *in vivo*. This loss was evenly distributed across single, branched, and multisynaptic spines, and did not account for the LTP-induced spinogenesis, which reached a greater level than PF at P15. Responses to test pulses also differed between P15 and more mature animals where at P55-70 the test pulse stimulation had an opposite effect, resulting in the recovery of small dendritic spines to their *in vivo* levels by 120 min (Bourne and Harris, 2011; Bell et al., 2014). Test pulse stimulation had no effect on response amplitude in adults; however, in developing animals even very low rates of stimulation can result in depressed responses within several minutes, relative to naïve responses (Abrahamsson et al., 2007; Cao and Harris, 2012). For these experiments, it was not possible to obtain strictly naïve responses because input/output curves were needed to establish uniform response magnitudes prior to TBS. Hence, it cannot be ruled out that the control test pulses produced response decrement relative to

naïve and then the ongoing test pulse stimulation eliminated weak or silent synapses.

Spinogenesis induced by TBS was not likely the result of perforation and splitting of pre-existing spine synapses (Toni et al., 1999; Luscher et al., 2000) for multiple reasons (Fiala et al., 2002a). First, the majority of spines at P15 had macular synapses and only a few of the largest synapses had perforated PSDs (i.e., fenestrated, horseshoe, or segmented shapes) (Geinisman et al., 1987). The large perforated synapses have more AMPA receptors and hence greater efficacy than macular synapses (Geinisman et al., 1987; Desmond and Weinberg, 1998). In the dentate gyrus of adult rats, more segmented PSDs occurred when high frequency stimulation, which elicited LTP, was delivered repeatedly for 4 days (Geinisman et al., 1991). In contrast, there were no sustained changes in perforated synapses following TBS in adult hippocampal area CA1 (Bourne and Harris, 2011). Similarly, at P15, there were no sustained changes in the density or sizes of perforated synapses following TBS-induced LTP. Second, branched spines with two heads sharing the same presynaptic axonal bouton were extremely rare, suggesting they also arose from spine outgrowth, not splitting. Third, if large synapses were splitting during LTP, their density should have decreased in parallel with the increase in spine number, which did not occur.

Induction of LTP results in the rapid conversion of silent synapses, with NMDA only responses, to active synapses (Liao et al., 1995; Isaac et al., 1995). These observations are consistent with the results at 5 min following the induction of LTP, where some spine heads enlarged and some spines elongated at P15. Enhanced stabilization of the AMPA receptors might explain why the new dendritic spines first detected at 30 min were sustained for 120 min. However, such spine stabilization probably did not result in further synaptic strengthening, because the potentiation was not elevated at 120 min, beyond the 5 min level. The small size of the new spines and synapses supports this hypothesis, because AMPA receptor density is well-correlated with total synapse area (Baude et al., 1995; Nusser, 2000; Nicholson and Geinisman, 2009). Further work is needed to determine whether the added spines between 30 and 120 min are also silent synapses.

Maintenance of net synaptic input by homeostatic synaptic scaling occurs in a variety of systems (Turrigiano, 2012). Compensatory synaptogenesis and LTP provide classic examples of homeostatic structural synaptic scaling. In hippocampal slices from mature but not developing hippocampus, compensatory synaptogenesis occurs when all synaptic transmission is blocked (Kirov et al., 1999; Kirov and Harris, 1999; Kirov et al., 2004; Petrak et al., 2005). Such regulation has also been observed in other systems suggesting that homeostatic synaptic scaling is intrinsic to the level of network activity at particular times during development (Desai et al., 2002; Turrigiano and Nelson, 2004; Maffei and Turrigiano, 2008a; Maffei and Turrigiano, 2008b). In adult hippocampus, the enlargement of some synapses following induction of LTP was balanced by disruption of test pulse-induced synaptogenesis (Bourne and Harris, 2011; Bell et al., 2014). In adults, neither the synapse enlargement nor the test pulse-induced synaptogenesis were evident until 120 min. Instead, presynaptic vesicles were recruited to nascent zones (portions of the PSD areas previously without presynaptic vesicles), converting them to active zones by 30 min after LTP induction. Subsequent growth of nascent zones occurred as synapses enlarged by 120 min after induction of LTP, despite no change in the level of potentiation (Bell et al., 2014). Thus, LTP-induced synaptic enlargement and test pulse-induced recovery of synapse number in adults, and conversely LTP-induced addition and test pulse-induced loss of synapses at P15, must all be silent processes. Furthermore, the absence of homeostatic compensation at P15 suggests LTP accelerates ongoing synaptogenesis because overall connectivity has not reached an adult, steady-state level.

Our data demonstrate that dendrites from developing and mature hippocampus respond to the same TBS protocol differently. At adult ages, when total synaptic density has plateaued, structural synaptic scaling is apparently accomplished by redistributing core dendritic resources to enlarged synapses, thereby preventing new spine formation. At a time when synaptogenesis is still prominent along developing dendrites, resource distribution could favor synaptogenesis instead of synapse enlargement. Polyribosomes, smooth endoplasmic reticulum, Golgi apparati, and endosomal compartments are highly dynamic in dendrites, and future investigations of their contributions to synaptogenesis versus synapse enlargement would provide valuable insights into the basic mechanisms of synapse regulation (Ostroff et al., 2002; Park et al., 2006; Bourne et al., 2007; Bourne and Harris, 2011; Cui-Wang et al., 2012). Like the enlarged synapses in adults, which have added nascent zones (i.e., quiet PSD area) during LTP (Bell et al., 2014), the new spines added following the induction of LTP by TBS at P15 also appear to have silent or weak synapses, because the level of potentiation was stable. Whether the newly enlarged (adult) or newly formed (P15) synapses are capable of recruiting dendritic resources during subsequent augmentation of LTP (Cao and Harris, 2012; Cao and Harris, 2014) is also an exciting prospect for future investigation.

Acknowledgments

We thank Libby Perry, Robert Smith, and John Mendenhall for technical assistance with the electron microscopy. LO and KH designed the experiments; LO and GC performed the slice electrophysiology; DJW, LO, PHP, HS, and KMH completed the 3D reconstructions; DJW and KMH performed the statistical analyses and wrote the paper. All co-authors provided editorial input. We thank members of the Harris Laboratory for insightful discussions.

REFERENCES

Abrahamsson T, Gustafsson B, Hanse E. 2007. Reversible synaptic depression in developing rat CA3 CA1 synapses explained by a

novel cycle of AMPA silencing–unsilencing. J Neurophysiol 98: 2604–2611.
Abrahamsson T, Gustafsson B, Hanse E. 2008. AMPA silencing is a prerequisite for developmental long-term potentiation in the hippocampal CA1 region. J Neurophysiol 100:2605–2614.
Baude A, Nusser Z, Molnar E, McIlhinney RA, Somogyi P. 1995. High-resolution immunogold localization of AMPA type glutamate receptor subunits at synaptic and non-synaptic sites in rat hippocampus. Neuroscience 69:1031–1055.
Bell ME, Bourne JN, Chirillo MA, Mendenhall JM, Kuwajima M, Harris KM. 2014. Dynamics of nascent and active zone ultrastructure as synapses enlarge during long-term potentiation in mature hippocampus. J Comp Neurol 522:3861–3884.
Bourne JN, Harris KM. 2008. Balancing structure and function at hippocampal dendritic spines. Annu Rev Neurosci 31:47–67.
Bourne JN, Harris KM. 2011. Coordination of size and number of excitatory and inhibitory synapses results in a balanced structural plasticity along mature hippocampal CA1 dendrites during LTP. Hippocampus 21:354–373.
Bourne JN, Sorra KE, Hurlburt J, Harris KM. 2007. Polyribosomes are increased in spines of CA1 dendrites 2 h after the induction of LTP in mature rat hippocampal slices. Hippocampus 17:4.
Bowden JB, Mendenhall JM, Abraham WC, Harris KM. 2008. Microtubule number as a correlate of dendritic spine density in dentate granule cells. Soc Neurosci Abstr 636.20.
Buzsaki G. 2002. Theta oscillations in the hippocampus. Neuron 33: 325–340.
Cao G, Harris KM. 2012. Developmental regulation of the late phase of long-term potentiation (L-LTP) and metaplasticity in hippocampal area CA1 of the rat. J Neurophysiol 107:902–912.
Cao G, Harris KM. 2014. Augmenting saturated LTP by broadly spaced episodes of theta-burst stimulation in hippocampal area CA1 of adult rats and mice. J Neurophysiol. pii: jn.00297.2014. [Epub ahead of print].
Colgan LA, Yasuda R. 2014. Plasticity of dendritic spines: Subcompartmentalization of signaling. Annu Rev Physiol 76:365–385.
Cui-Wang T, Hanus C, Cui T, Helton T, Bourne J, Watson D, Harris KM, Ehlers MD. 2012. Local zones of endoplasmic reticulum complexity confine cargo in neuronal dendrites. Cell 148:309–321.
Desai NS, Cudmore RH, Nelson SB, Turrigiano GG. 2002. Critical periods for experience-dependent synaptic scaling in visual cortex. Nat Neurosci 5:783–789.
Desmond NL, Weinberg RJ. 1998. Enhanced expression of AMPA receptor protein at perforated axospinous synapses. Neuroreport 9: 857–860.
Ehrlich I, Klein M, Rumpel S, Malinow R. 2007. PSD-95 is required for activity-driven synapse stabilization. Proc Natl Acad Sci USA 104:4176–4181.
Engert F, Bonhoeffer T. 1999. Dendritic spine changes associated with hippocampal long-term synaptic plasticity. Nature 399:66–70.
Fiala JC. 2005. Reconstruct: A free editor for serial section microscopy. J Microsc 218:52–61.
Fiala JC, Allwardt B, Harris KM. 2002a. Dendritic spines do not split during hippocampal LTP or maturation. Nat Neurosci 5:297–298.
Fiala JC, Feinberg M, Popov V, Harris KM. 1998. Synaptogenesis via dendritic filopodia in developing hippocampal area CA1. J Neurosci 18:8900–8911.
Fiala JC, Harris KM. 2001a. Cylindrical diameters method for calibrating section thickness in serial electron microscopy. J Microsc 202:468–472.
Fiala JC, Harris KM. 2001b. Extending unbiased stereology of brain ultrastructure to three-dimensional volumes. J Am Med Inform Assoc 8:1–16.
Fiala JC, Harris KM. 2002. Computer-based alignment and reconstruction of serial sections. Microsc Anal 87:5–8.
Fiala JC, Kirov SA, Feinberg MD, Petrak LJ, George P, Goddard CA, Harris KM. 2003. Timing of neuronal and glial ultrastructure disruption during brain slice preparation and recovery *in vitro*. J Comp Neurol 465:90–103.
Fiala JC, Spacek J, Harris KM. 2002b. Dendritic spine pathology: Cause or consequence of neurological disorders? Brain Res Brain Res Rev 39:29–54.
Geinisman Y, Morrell F, de Toledo-Morrell L. 1987. Axospinous synapses with segmented postsynaptic densities: A morphologically distinct synaptic subtype contributing to the number of profiles of 'perforated' synapses visualized in random sections. Brain Res 423: 179–188.
Geinisman Y, Toledo-Morrell L, Morrell F. 1991. Induction of long-term potentiation is associated with an increase in the number of axospinous synapses with segmented postsynaptic densities. Brain Res 566:77–88.
Gulledge AT, Carnevale NT, Stuart GJ. 2012. Electrical advantages of dendritic spines. PLoS One 7:e36007.
Harnett MT, Makara JK, Spruston N, Kath WL, Magee JC. 2012. Synaptic amplification by dendritic spines enhances input cooperativity. Nature 491:599–602.
Harris KM. 1999. Structure, development, and plasticity of dendritic spines. Curr Opin Neurobiol 9:343–348.
Harris KM, Bourne JN, Mendenhall JM, Spacek J. 2007. Hippocampal CA1 dendrites of greater caliber have more spines and contain more microtubules as a subcellular supply route. Soc Neurosci Abstr 147.19.
Harris KM, Jensen FE, Tsao B. 1992. Three-dimensional structure of dendritic spines and synapses in rat hippocampus (CA1) at postnatal day 15 and adult ages: Implications for the maturation of synaptic physiology and long-term potentiation. J Neurosci 12: 2685–2705.
Harris KM, Perry E, Bourne J, Feinberg M, Ostroff L, Hurlburt J. 2006. Uniform serial sectioning for transmission electron microscopy. J Neurosci 26:12101–12103.
Harris KM, Spacek J, Bell ME, Parker PH, Lindsey LF, Baden AD, Vogelstein JT, Burns R. 2015. A resource from 3D electron microscopy of hippocampal neuropil for user training and tool development. Sci Data 2:150046.
Harris KM, Teyler TJ. 1984. Developmental onset of long-term potentiation in area CA1 of the rat hippocampus. J Physiol 346: 27–48.
Harris KM, Weinberg RJ. 2012. Ultrastructure of synapses in the mammalian brain. In: Sheng M, Sabatini BL, Südhof TC, editors. The Synapse. Cold Spring Harbor, NY: Cold Spring Harbor Laboratory Press. pp 1–30. Cold Spring Har Perspect Biol. doi: 10.1101/cshperspect.a005587.
Isaac JT, Nicoll RA, Malenka RC. 1995. Evidence for silent synapses: Implications for the expression of LTP. Neuron 15:427–434.
Isomura Y, Kato N. 1999. Action potential-induced dendritic calcium dynamics correlated with synaptic plasticity in developing hippocampal pyramidal cells. J Neurophysiol 82:1993–1999.
Jackson PS, Suppes T, Harris KM. 1993. Stereotypical changes in the pattern and duration of long-term potentiation expressed at postnatal days 11 and 15 in the rat hippocampus. J Neurophysiol 70: 1412–1419.
Jensen FE, Harris KM. 1989. Preservation of neuronal ultrastructure in hippocampal slices using rapid microwave-enhanced fixation. J Neurosci Methods 29:217–230.
Kirov SA, Goddard CA, Harris KM. 2004. Age-dependence in the homeostatic upregulation of hippocampal dendritic spine number during blocked synaptic transmission. Neuropharmacology 47: 640–648.
Kirov SA, Harris KM. 1999. Dendrites are more spiny on mature hippocampal neurons when synapses are inactivated. Nat Neurosci 2:878–883.
Kirov SA, Sorra KE, Harris KM. 1999. Slices have more synapses than perfusion-fixed hippocampus from both young and mature rats. J Neurosci 19:2876–2886.

Kisvarday ZF, Gulyas A, Beroukas D, North JB, Chubb IW, Somogyi P. 1990. Synapses, axonal and dendritic patterns of GABA-immunoreactive neurons in human cerebral cortex. Brain 113 (Pt 3):793–812.

Kopec CD, Li B, Wei W, Boehm J, Malinow R. 2006. Glutamate receptor exocytosis and spine enlargement during chemically induced long-term potentiation. J Neurosci 26:2000–2009.

Kopec CD, Real E, Kessels HW, Malinow R. 2007. GluR1 links structural and functional plasticity at excitatory synapses. J Neurosci 27:13706–13718.

Kramar EA, Lynch G. 2003. Developmental and regional differences in the consolidation of long-term potentiation. Neuroscience 118: 387–398.

Kuwajima M, Mendenhall JM, Harris KM. 2013a. Large-volume reconstruction of brain tissue from high-resolution serial section images acquired by SEM-based scanning transmission electron microscopy. Methods Mol Biol 950:253–273.

Kuwajima M, Spacek J, Harris KM. 2013b. Beyond counts and shapes: Studying pathology of dendritic spines in the context of the surrounding neurophil through serial section electron microscopy. Neurosci 251:75–89.

Lee SJ, Escobedo-Lozoya Y, Szatmari EM, Yasuda R. 2009. Activation of CaMKII in single dendritic spines during long-term potentiation. Nature 458:299–304.

Liao D, Hessler NA, Malinow R. 1995. Activation of postsynaptically silent synapses during pairing-induced LTP in CA1 region of hippocampal slice. Nature 375:400–404.

Lin YC, Koleske AJ. 2010. Mechanisms of synapse and dendrite maintenance and their disruption in psychiatric and neurodegenerative disorders. Annu Rev Neurosci 33:349–378.

Luscher C, Nicoll RA, Malenka RC, Muller D. 2000. Synaptic plasticity and dynamic modulation of the postsynaptic membrane. Nat Neurosci 3:545–550.

Maffei A, Turrigiano G. 2008a. The age of plasticity: Developmental regulation of synaptic plasticity in neocortical microcircuits. Prog Brain Res 169:211–223.

Maffei A, Turrigiano GG. 2008b. Multiple modes of network homeostasis in visual cortical layer 2/3. J Neurosci 28:4377–4384.

Maletic-Savatic M, Malinow R, Svoboda K. 1999. Rapid dendritic morphogenesis in CA1 hippocampal dendrites induced by synaptic activity. Science 283:1923–1927.

Matsuzaki M, Honkura N, Ellis-Davies GC, Kasai H. 2004. Structural basis of long-term potentiation in single dendritic spines. Nature 429:761–766.

Meyer D, Bonhoeffer T, Scheuss V. 2014. Balance and stability of synaptic structures during synaptic plasticity. Neuron 82:430–443.

Morgan SL, Teyler TJ. 2001. Electrical stimuli patterned after the theta-rhythm induce multiple forms of LTP. J Neurophysiol 86: 1289–1296.

Nguyen PV, Kandel ER. 1997. Brief theta-burst stimulation induces a transcription-dependent late phase of LTP requiring cAMP in area CA1 of the mouse hippocampus. Learn Mem 4:230–243.

Nicholson DA, Geinisman Y. 2009. Axospinous synaptic subtype-specific differences in structure, size, ionotropic receptor expression, and connectivity in apical dendritic regions of rat hippocampal CA1 pyramidal neurons. J Comp Neurol 512:399–418.

Nusser Z. 2000. AMPA and NMDA receptors: Similarities and differences in their synaptic distribution. Curr Opin Neurobiol 10:337–341.

Nusser Z, Sieghart W, Benke D, Fritschy JM, Somogyi P. 1996. Differential synaptic localization of two major gamma-aminobutyric acid type A receptor alpha subunits on hippocampal pyramidal cells. Proc Natl Acad Sci USA 93:11939–11944.

Oh WC, Parajuli LK, Zito K. 2015. Heterosynaptic structural plasticity on local dendritic segments of hippocampal CA1 neurons. Cell Rep 10:162–169.

Ostroff LE, Fiala JC, Allwardt B, Harris KM. 2002. Polyribosomes redistribute from dendritic shafts into spines with enlarged synapses during LTP in developing rat hippocampal slices. Neuron 35: 535–545.

Park M, Penick EC, Edwards JG, Kauer JA, Ehlers MD. 2004. Recycling endosomes supply AMPA receptors for LTP. Science 305: 1972–1975.

Park M, Salgado JM, Ostroff L, Helton TD, Robinson CG, Harris KM, Ehlers MD. 2006. Plasticity-induced growth of dendritic spines by exocytic trafficking from recycling endosomes. Neuron 52:817–830.

Penzes P, Cahill ME, Jones KA, VanLeeuwen JE, Woolfrey KM. 2011. Dendritic spine pathology in neuropsychiatric disorders. Nat Neurosci 14:285–293.

Petrak LJ, Harris KM, Kirov SA. 2005. Synaptogenesis on mature hippocampal dendrites occurs via filopodia and immature spines during blocked synaptic transmission. J Comp Neurol 484:183–190.

Raymond CR, Redman SJ. 2002. Different calcium sources are narrowly tuned to the induction of different forms of LTP. J Neurophysiol 88:249–255.

Raymond CR, Redman SJ. 2006. Spatial segregation of neuronal calcium signals encodes different forms of LTP in rat hippocampus. J Physiol 570:97–111.

Reynolds ES. 1963. The use of lead citrate at high pH as an electron-opaque stain in electron microscopy. J Cell Biol 17:208–212.

Somogyi P, Fritschy JM, Benke D, Roberts JD, Sieghart W. 1996. The gamma 2 subunit of the GABAA receptor is concentrated in synaptic junctions containing the alpha 1 and beta 2/3 subunits in hippocampus, cerebellum and globus pallidus. Neuropharmacology 35:1425–1444.

Sorra KE, Fiala JC, Harris KM. 1998. Critical assessment of the involvement of perforations, spinules, and spine branching in hippocampal synapse formation. J Comp Neurol 398:225–240.

Sorra KE, Harris KM. 1998. Stability in synapse number and size at 2 hr after long-term potentiation in hippocampal area CA1. J Neurosci 18:658–671.

Staubli U, Lynch G. 1987. Stable hippocampal long-term potentiation elicited by 'theta' pattern stimulation. Brain Res 435:227–234.

Takasaki K, Sabatini BL. 2014. Super-resolution 2-photon microscopy reveals that the morphology of each dendritic spine correlates with diffusive but not synaptic properties. Front Neuroanat 8:29.

Tominaga-Yoshino K, Urakubo T, Okada M, Matsuda H, Ogura A. 2008. Repetitive induction of late-phase LTP produces long-lasting synaptic enhancement accompanied by synaptogenesis in cultured hippocampal slices. Hippocampus 18:281–293.

Toni N, Buchs PA, Nikonenko I, Bron CR, Muller D. 1999. LTP promotes formation of multiple spine synapses between a single axon terminal and a dendrite. Nature 402:421–425.

Tonnesen J, Katona G, Rozsa B, Nagerl UV. 2014. Spine neck plasticity regulates compartmentalization of synapses. Nat Neurosci 17: 678–685.

Turrigiano G. 2012. Homeostatic synaptic plasticity: Local and global mechanisms for stabilizing neuronal function. Cold Spring Harb Perspect Biol 4:a005736.

Turrigiano GG. 2008. The self-tuning neuron: Synaptic scaling of excitatory synapses. Cell 135:422–435.

Turrigiano GG, Nelson SB. 2004. Homeostatic plasticity in the developing nervous system. Nat Rev Neurosci 5:97–107.

Yang Y, Takeuchi K, Rodenas-Ruano A, Takayasu Y, Bennett MV, Zukin RS. 2009. Developmental switch in requirement for PKA RIIbeta in NMDA-receptor-dependent synaptic plasticity at Schaffer collateral to CA1 pyramidal cell synapses. Neuropharmacology 56:56–65.

Yasuda H, Barth AL, Stellwagen D, Malenka RC. 2003. A developmental switch in the signaling cascades for LTP induction. Nat Neurosci 6:15–16.